Heliyon 10 (2024) e28307

Contents lists available at ScienceDirect

Heliyon

journal homepage: www.cell.com/heliyon

Research article

Development and validation of a novel prognostic lncRNA signature based on the APOBEC3 family genes in gastric cancer

Jia Qi [a,1], Wenxuan Wu [a,1], Jing Chen [a], Xiaying Han [a], Zhixing Hao [a], Yaxuan Han [a], Yewei Xu [a], Jun Lai [b,**], Jian Chen [a,*]

[a] Department of Gastrointestinal Surgery, The Second Affiliated Hospital, Zhejiang University School of Medicine, Hangzhou, 310000, Zhejiang, China

[b] Department of Cardiology Guangdong Second Provincial General Hospital, Guangzhou, 510000, Guangdong, China

ARTICLE INFO

Keywords:
Gastric cancer
APOBEC3-Related lncRNA prognostic signature
Nomogram
Mutation
Immune checkpoints
Therapy decision

ABSTRACT

Introduction: Gastric Cancer (GC) refers to a prevalent malignant cancer accompanied by a weak prognosis. The APOBEC3 family genes and lncRNAs are linked with cancer progression. Nevertheless, there is still a scarcity of data concerning the prognostic value of APOBEC3-related lncRNAs in GC.

Methods: We extracted the data from GC samples, including transcriptome as well as clinical data, obtained from the TCGA database. Then, we screened for lncRNAs that were correlated with the APOBEC3 family genes and constructed an APOBEC3-related lncRNA prognostic signature (LPS) by utilizing univariate Cox and lasso regression analysis. Furthermore, we validated our constructed signature and evaluated it thoroughly, including analysis of its function, immunity, mutations, and clinical applications via multiple methods, including Metascape, GSEA, and analyses including TIC and TME, immune checkpoints, CNV and SNPs, Kaplan-Meier survival curves, nomogram, decision tree and drug prediction analysis. Finally, we overexpressed LINC01094 to evaluate the impacts on the proliferation as well as migration with regards to KATO-2 cells.

Results: We selected eight lncRNAs for our APOBEC3-related LPS, which is demonstrated as a valuable tool in predicting the individual GC patients' prognosis. Subsequently, we segregated the samples into subgroups of high-as well as low-risk relying on the risk score with regards to APOBEC3-related LPS. By performing functional analysis, we have shown that immune-as well as tumor-related pathways were enriched in high- and low-risk GC patients. Furthermore, immune analysis revealed a robust correlation between the APOBEC3-related LPS and immunity. We found that immune checkpoints were significantly associated with the APOBEC3-related LPS and were greatly exhibited in GC tumor and high-risk samples. Mutational analysis suggested that the mutational rate was greater in low-risk samples. Furthermore, we predicted small molecular drugs displayed greater sensitivity in patients categorized as high-risk. Moreover, the immune response was also better in high-risk patients. Of these drugs, dasatinib was significant in both methods and might be considered a potential novel drug for treating high-risk GC patients. Finally, we found that LINC01094 has the potential to enhance the migration, proliferation as

* Corresponding author.
** Corresponding author.
E-mail addresses: Jun123zm@163.com (J. Lai), zrchenjian@zju.edu.cn (J. Chen).
[1] These authors share first authorship.

https://doi.org/10.1016/j.heliyon.2024.e28307
Received 29 December 2023; Received in revised form 15 March 2024; Accepted 15 March 2024
Available online 17 March 2024
2405-8440/© 2024 The Authors. Published by Elsevier Ltd. This is an open access article under the CC BY-NC license (http://creativecommons.org/licenses/by-nc/4.0/).

well as inhibit apoptosis of KATO-2 in GC cells. And Dasatinib has an inhibitory effect on the migration as well as proliferation in GC cells.
Conclusion: We created a novel APOBEC3-related LPS in predicting the prognosis with regards to individual GC patients. Importantly, this APOBEC3-related LPS was closely associated with immunity and might guide clinical treatment.

1. Introduction

Gastric cancer (GC) positions as the 5th most prevalent malignant cancer as well as the third primary cause with regards to cancer-related mortality globally [1]. According to clinical data, GC has a weak prognosis; and only 10–25% of GC patients survive long-term in Europe and the USA [2]. Unfortunately, the treatment methods for GC are currently limited, and while the mainstay of treatment is chemotherapy, patient responses to chemotherapy are not satisfactory. The patient's median overall survival (OS) with evolved GC is less than 13–17 months in Japan/East Asia as well as 8–11 months in the Western world [3].

The human apolipoprotein B mRNA editing enzyme catalytic polypeptide-like 3 (APOBEC3) family genes comprises seven members, including APOBEC3A-D and APOBEC3F–H, which are all located on human chromosome 22 [4]. APOBEC3 family members are often deregulated in cancer cells which ultimately result in mutations [5]. Recent studies have illustrated that mutations in the APOBEC3 family genes are associated with cancer risk in many cancer types [6–8]. Moreover, the undesirable activity of the APOBEC3 family genes is related to the development of cancer [9]. Nevertheless, research on APOBEC3 family members in gastric cancer remains limited. Hence, the objective of the current research was to discover the importance of APOBEC3 family members in gastric cancer.

Long noncoding RNAs (lncRNAs) are comprised of more than 200 nucleotides as well as primarily non-encoding proteins [10]. Several lncRNAs have been extensively researched with regards to its purpose, which involves regulating genes, chromatin dynamics, growth, development and cell differentiation [11]. The advent of next-generation sequencing has unveiled that more than thousands of lncRNAs are abnormally expressed in numerous cancers [12]. Crucially, numerous lncRNAs have been demonstrated to be linked to the prognosis of various cancer types and possible therapeutic targets [13–15].

With regards to our previous research, we revealed the relationship between lncRNA H19 and APOBEC3G, which is one of the members of the APOBEC3 family [16]. Thus, we were curious about whether APOBEC3-related lncRNAs can serve as a novel prognostic signature in GC. In current research, we used bioinformatic analysis in constructing a novel APOBEC3-related lncRNA prognostic signature (LPS) for GC. Furthermore, we performed thorough mutational, immune, functional and clinical analyses to assess this APOBEC3-related lncRNA prognostic signature. Finally, therapy decision analysis was performed to guide clinical drug selection. A flowchart outlining our investigation is illustrated in Suppl. Fig. S1.

2. Methods

2.1. Data extraction from the TCGA database

The transcriptome RNA sequencing data of 407 samples, including 32 paragastric cancer tissues and 375 gastric tissues, were gained by downloading them from The Cancer Genome Atlas (TCGA) (https://portal.gdc.cancer.gov/); as a result, the expression levels of a total of 56,530 genes were extracted. Clinical data extracted from gastric cancer patients were acquired from the TCGA database as well. The Illumina Human Methylation 450 cohort was downloaded from UCSC Xena's online exploration tool (https://xena.ucsc.edu/).

2.2. Mutation analysis

The R package "TCGAbiolinks" was utilized for downloading the GC patients' mutation data in maf format from the TCGA database. Moreover, the mutation data were further examined by the R package "maftools". As a result, the tumor mutational burden (TMB) concerning the GC samples was computed, while the mutational landscape was obtained. Moreover, the mutational spectrum of mutational signatures (MutSig) was ascertained using the R package "deconstructSigs". The humor-related mutational signatures (COSMIC Signatures 1 and 5) as well as APOBEC-related mutational signatures (COSMIC Signatures 2 and 13) were involved in the analysis.

For copy number alteration (CNA) analysis, we downloaded CNA data from GC patients from UCSC Xena's online exploration tool (https://xena.ucsc.edu/). Subsequently, the computational approach to the genomic identification of significant targets in cancer (GISTIC 2.0) was utilized for evaluation under the following thresholds: amplification (AMP) > 0.3; deletion (Del) < -0.3.

3. Establishment of the APOBEC3-related LPS

All lncRNAs were derived from transcriptome data. The correlation between seven APOBEC3 family genes as well as lncRNAs was examined by Pearson's test. The threshold was set as follows: Pearson correlation >0.3 or < -0.3, P value less than 0.001. The correlation network was generated by Cytoscape (3.8.0) and visualized by cytoHubba. To screen for prognostic lncRNAs, univariate Cox regression analysis was performed (P value less than 0.05). A forest plot was obtained by using R studio. The R package "pheatmap"

was utilized in order to construct a heatmap with regards to the expression of lncRNAs between normal as well as tumor samples. To establish the APOBEC3-related LPS, we conducted selection operator (LASSO) regression as well as least absolute shrinkage. The corresponding coefficients (β) concerning the APOBEC3-related LPS were acquired. The risk score, which was constructed from the APOBEC3-related LPS, was computed using the formula below:

Risk score $= \sum [\text{expression}(\text{APOBEC3-related LPS}) * \beta]$.

3.1. Validation of the APOBEC3-related LPS

After randomly splitting samples into training as well as testing cohorts at a ratio of 1:1, the significance of the APOBEC3-related LPS in the two cohorts was validated by Kaplan-Meier (K-M) analysis utilizing the R package "survival" in R studio. An analysis of area under the curve (AUC) was performed to evaluate the APOBEC3-related LPS reliability utilizing the R package "timeROC". Furthermore, to evaluate whether the APOBEC3-related LPS could be a prognostic marker, we conducted both multivariate as well as univariate Cox regression analyses in both cohorts.

3.2. Construction of a nomogram relying on the APOBEC3-related LPS

According to the univariate Cox regression analysis with regards to the APOBEC3-related LPS and the clinical data extracted from the TCGA database, we developed a nomogram to forecast the 1-, 3- as well as 5-year OS of GC patients using the "RMS" package in R studio. In order to verify the superiority as well as accuracy of this nomogram further, we constructed a calibration curve and performed AUC analysis using the "rms" as well as "survivalROC" packages. Moreover, 1-, 3- and 5-year decision curve analysis (DCA) was conducted in comparing the net benefits of the constructed nomogram utilizing the R package "rmda".

3.3. Functional enrichment analysis

After obtaining the differentially expressed genes among the high-as well as low-risk samples by employing the R package "limma" in R studio, we used the online gene annotation as well as analysis resource Metascape to analyze the function of the APOBEC3-related LPS. Gene set enrichment analysis (GSEA) (4.1.0) was employed in determining the functional enrichment of all samples relying on the risk score derived from the APOBEC3-related LPS. For the functional enrichment analysis with regards to tumor-infiltrating immune cells (TICs), the R package "cibersortR" was used to calculate every immune cell's relative abundance in each sample. Meanwhile, the immune-related pathways were determined from a prior article [17]. According to McDermott [18], the molecular signatures of angiogenesis, immunity (including the T-effector/IFN- response as well as checkpoint) as well as myeloid inflammation were obtained. Similarly, signatures of epithelial-mesenchymal transition (EMT) [19] and the hypoxia [20] were gained. Afterward, we utilized the R package "gsva" in assessing the enrichment score of the samples in different pathways we determined by performing ssGSEA.

3.4. Immune analysis of the APOBEC3-related LPS

We performed cluster analysis of 22 TICs and assessed their correlations with Pearson's correlation analysis, with significance determined by P values less than 0.01. Univariate Cox regression analysis was conducted to pinpoint the cells linked to prognosis. For the analysis with regards to the tumor microenvironment (TME) anal, the stromal, immune as well as ESTIMATES scores for each sample were calculated.

Relying on their Pearson correlation coefficients, we sorted the six common immune checkpoints from PubMed and evaluated the correlation between these checkpoints as well as the APOBEC3-related LPS. The relative expression of the six common immune checkpoints in GC along with normal samples and in high-as well as low-risk patients was analyzed.

3.5. Prediction of sensitivity to chemotherapy and potential small-molecule drugs

Based on the genomics of drug sensitivity in cancer (GDSC) database (www.cancerRxgene.org), we conducted a ridge regression analysis to evaluate the half-maximal inhibitory concentration (IC50) of three common GC chemo-drugs in the high-as well as low-risk samples via the R package "pRRophetic".

We included two databases in our analyses. The Cancer Therapeutics Response Portal (CTRP) version 2.0 contains data on the sensitivity of 860 cancer cell lines (CCLs) to 481 small-molecule drugs. The PRISM (profiling relative inhibition simultaneously in mixtures) database offers a web-based analysis platform for the high-throughput screening of numerous drugs across hundreds of human CCLs, offering analysis at a scale unmatched previously. We used the CTRP 2.0 (http://portals.broadinstitute.org/ctrp/) as well as PRISM (https://www.theprismlab.org/) databases to predict the potential sensitivities of small-molecule drugs. The AUC serves as a standard metric in assessing the drug sensitivity, where a smaller AUC value indicates enhanced drug sensitivity. The expression data for CCLs were retrieved from the Cancer Cell Line Encyclopedia (CCLE) (https://portals.broadinstitute.org/ccle/). Based on the expression data with regards to these CCLs and from the TCGA, we established a ridge regression model in predicting the sensitivity of drugs in different risk scores by utilizing the R package "pRRophetic".

Since the differentially expressed genes among high-as well as low-risk patients might act as potential targets for GC treatment, we employed the database ConnectivityMap (cMap) (https://clue.io/) to explore prospective drugs that targeted the differentially expressed genes. Relying on the cMap database, we uncovered the mechanism of action (MoA) of the predicted drugs for GC patients.

3.6. Prediction of response to immunotherapy

We applied the developed tumor immune dysfunction and exclusion (TIDE) model (http://tide.dfci.harvard.edu) [21] to foresee the response to the treatment against PD-1 and CTLA in GC patients. TIDE is a well-known enrichment algorithm that has been widely employed in cancer-related study [22–25]. Afterward, we compared the existing dataset, which includes the treatment response to PD-1 as well as CTLA4 in 47 patients [26] using subclass mapping (https://cloud.genepattern.org/gp/) [27]. This comparison successfully predicted the immune response in high as well as low-risk GC patients.

3.7. Cell culture and treatment

Human gastric cancer cells KATO (GDC0253) were procured from Taze Biotech (Shanghai, China). Note that the cells were cultured in DMEM consisting of 10% FBS as well as the medium was renewed up until the cell concentration reached 85%. Experiments were conducted using cells from passages 3 to 10.

3.8. Cell proliferation

Cell viability after treating with puro and LINC01094 were assessed using the MTT assay. The cells were calculated prior to being plated into 96-well plates. After 48 h or 72 h of treatment, 10 μL MTT solution (5 mg/mL) was inserted to every well for 4 h proceeded with adding 150 μL dimethyl sulfoxide to every well which was then positioned on a low-speed shaker for 10 min to assure total dissolution of the crystals. Here, the absorbance was calculated to be OD490 nm by a microplate reader.

EDU kit was employed in measuring the cells proliferation in each group after transfection. The specific steps are: add 1 mL of EDU solution diluted with culture medium (culture medium: EDU solution = 1000:1), place at 37 °C for 2 h, discard the supernatant, and then add 200 μL of 4% paraformaldehyde to each well for fixation 30 min. Following the instructions of the EDU kit, add glycine solution (2 mg/mL) and Appollo staining solution to each well in turn. Subsequently, the nuclei were stained with DAPI for a duration of 30 min, which were then examined and captured utilizing a fluorescence microscope.

3.9. Cell migration

Cells were seeded in a 6-well culture plate to allow the formation of a confluent monolayer. Here, a scratch wound was instigated by utilizing a 1000 μl pipette tip. For debris removal, cells were washed using PBS as well as the culture medium was replaced. Images were acquired at 0 h and 24 h post-scratch. The wound size was calculated with Image J software.

3.10. Apoptosis TUNEL staining

The above-mentioned cells fixed in 4% paraformaldehyde were taken, and the apoptosis was detected by referring to the operation steps of the TUNEL apoptosis kit. Observed under a laser scanning confocal microscope, the apoptotic cells were fluorescent green.

3.11. qRT-PCR

Extract total RNA from cells with the use of Trizol reagent. Following this, perform reverse transcription employing the PrimeScript RT Reagent Kit. Then, follow the instructions of the SYBR Premix Ex *Taq*II Kit to conduct real-time fluorescence quantitative PCR amplification on the Applied Biosystems 7500 real-time PCR system (reference sequences see Table 1).

3.12. Statistical analysis

All statistical analyses including the creation of figures were carried out in R software (version 4.0.4). We used the Wilcoxon test to detect differences among the two groups. The proportions' differences were examined utilizing the chi-squared test. Moreover, a P value of less than 0.05 was deemed as statistically significant. Kaplan-Meier (KM) analysis was carried out to construct an OS curve for each subgroup. All correlation analyses were conducted using Pearson's correlations. A log-rank test was utilized to enlarge the significant differences. We utilized the R package "survival" in conducting univariate as well as multivariate Cox regression analyses. Furthermore, the R package "rpart" was utilized to develop the decision tree of *P less than 0.05, **P less than 0.01, ***P less than 0.001.

Table 1
The RT-PCR reference sequences.

Gene		Primer sequence
LINC01094	Forward	5′-TCCCTTCCACAGAGAAGGCT-3′
	Reverse	3′-AGGTTGACACATCTCGCCTG -5′

4. Results

4.1. Genomics landscape analysis of the APOBEC3 family genes

First, we explored the mutational profile of the APOBEC3 family genes in GC (Fig. 1). The samples were split according to the stage of GC patients. The spectrum of the tumor mutational burden (TMB) and mutation signature (MutSig) were illustrated. We found that four members (APOBEC3B, APOBEC3C, APOBEC3F and APOBEC3D) of the APOBEC3 family had single nucleotide variants (SNVs). Most of the mutations were observed at stage III, and no mutations were found at stage I. The CNA analysis found typical amplifications and deletions. For instance, amplification mutations in 7p22.1 (51%), 8q24.21 (70%), 8p23.1 (40%), 17q12 (33%), 19q12 (29%) and 20q13.2 (68%) were widely observed. Deletion mutations in 4q35.1 (48%), 5q12.1 (40%), 9p21.3 (46%), 9p23 (46%), 10q23.31 (27%), 16p13.3 (23%), 17p12 (42%), 18q12.2 (42%) and 18q21.2 (48%) were found in GC patients. At the gene level, 43% copy number alterations were detected in four APOBEC3 genes.

4.2. Eight lncRNAs were selected as APOBEC3-related prognostic signatures

From the TCGA database, 407 GC samples, including transcriptome profiling data and clinical data, were extracted. Fourteen thousand eighty-six lncRNAs were split from the transcriptome profiling data. Then, Pearson correlation analysis was conducted between the 7 APOBEC3 family members and the 14,086 lncRNAs with a threshold of $|Cor| < 0.3$ as well as P value < 0.001. We identified 268 APOBEC3-related lncRNAs. To determine the correlations among the 7 APOBEC3 family genes and the APOBEC3-related lncRNAs more directly, we performed a co-expression network with the use of Cytoscape (3.8.0) (Fig. 2A). Next, we conducted univariate Cox regression analysis to further select 10 APOBEC3-related prognostic lncRNAs (P value of less than 0.05) (Fig. 2B). In addition, we evaluated the expression with regards to the ten chosen lncRNAs in the GC samples and normal samples. Except for SENCR and PSMG3-AS1, which were downregulated, the remaining eight lncRNAs were upregulated in the GC sample (P value < 0.05) (Fig. 2C). We performed a Lasso regression and subsequently included these eight lncRNAs in the APOBEC3-related LPS according to the optimal value of lambda (0.01695552) (Fig. 2D). The coefficients of these eight APOBEC3-related prognostic lncRNAs

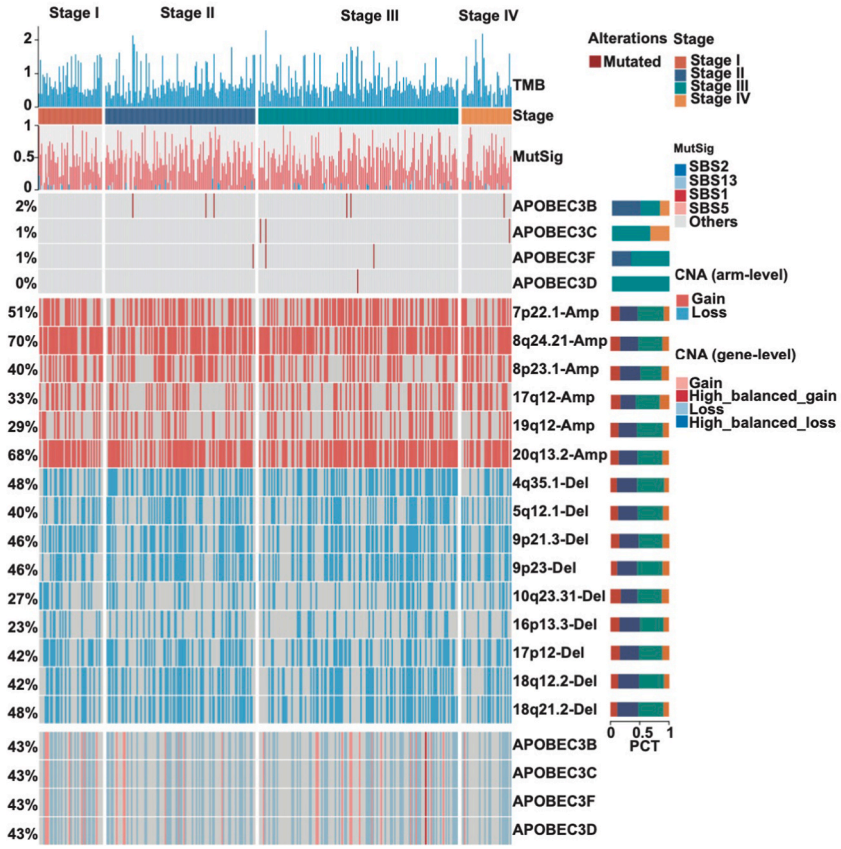

Fig. 1. Genomics mutation analysis of the APOBEC3 family genes. The mutational landscape of the APOBEC3 family genes is shown in different stages. The TMB and MutSig spectra were detected in each sample. The percentage of mutations in the APOBEC3 family genes is shown. The percentage and the location of amplifications and deletions was evaluated by CNA analysis.

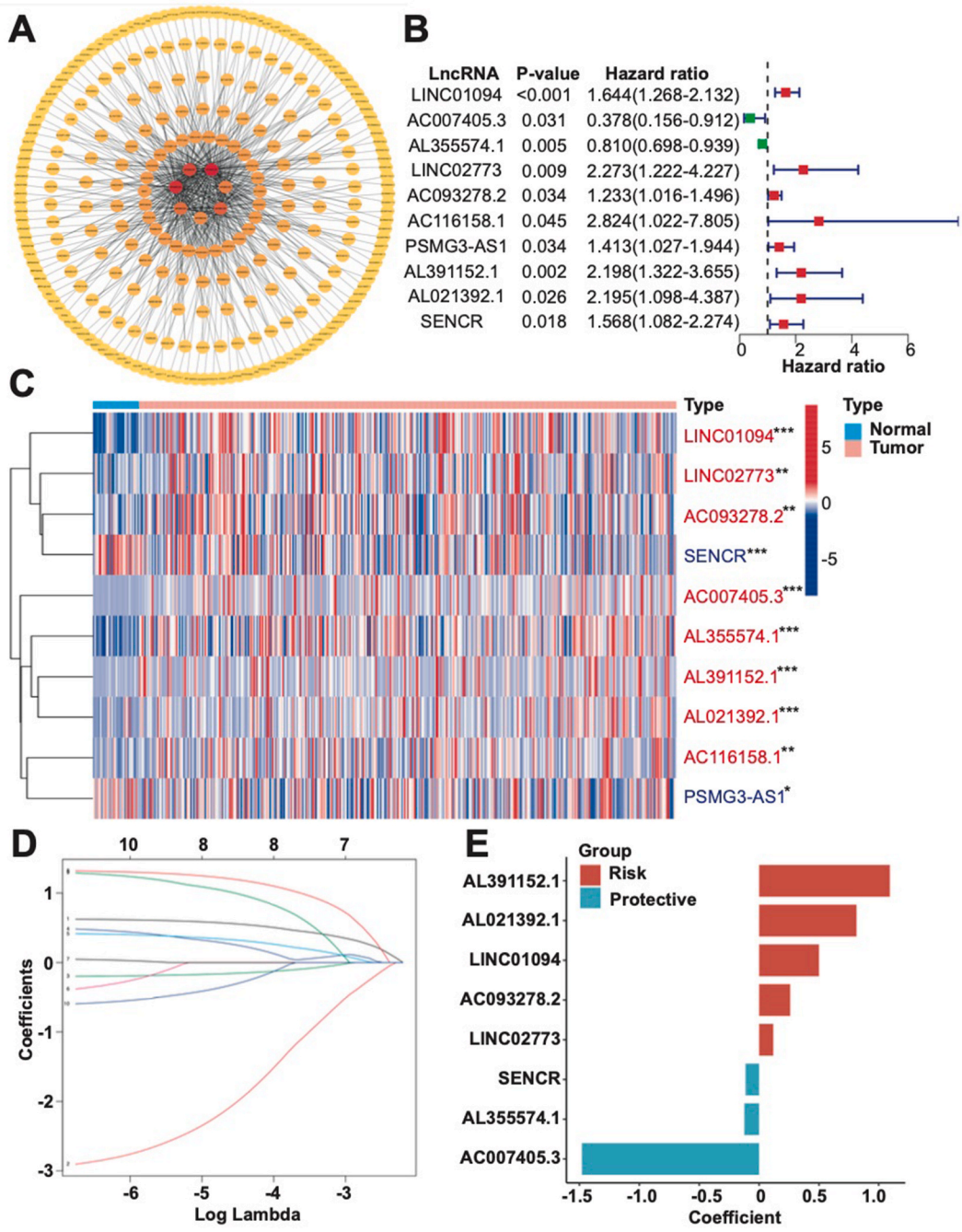

Fig. 2. Inclusion of 8 lncRNAs as APOBEC3-related prognostic signatures. (A) The network of the APOBEC3 family genes and the correlated lncRNAs (|Cor| < 0.3, P value < 0.001). (B) The prognostic APOBEC3-related lncRNAs are shown in a forest plot (P value < 0.05). (C) The expression of ten prognostic APOBEC3-related lncRNAs in GC and normal tissue is shown in the heatmap. Red represents high expression in GC, while blue represents low expression in GC. (D) Lasso regression analysis of ten prognostic APOBEC3-related lncRNAs. The X-axis represents Log Lambda, and the Y-axis represents coefficients. (E) The coefficient of the APOBEC3-related LPS. *P < 0.05, **P < 0.01, ***P < 0.001. (For interpretation of the references to colour in this figure legend, the reader is referred to the Web version of this article.)

are shown in Fig. 2E.

4.3. The APOBEC3-related LPS predicts the survival of GC patients

To evaluate the APOBEC3-related LPS, we segregated the GC samples at random into two cohorts (testing as well as training

cohorts) in a proportion of 1:1. Then we established the risk score with regards to the APOBEC-related LPS. The samples were segregated into two groups (the high-as well as low-risk groups) relying on the median value of the risk score. Moreover, by conducting Kaplan-Meier analysis, we demonstrated that the high-risk patients possessed a shorter survival in both the training (P value less than 0.001) as well as testing cohorts (P = 0.022) (Fig. 3A and B). Then, we evaluated the risk score for each sample within both cohorts.

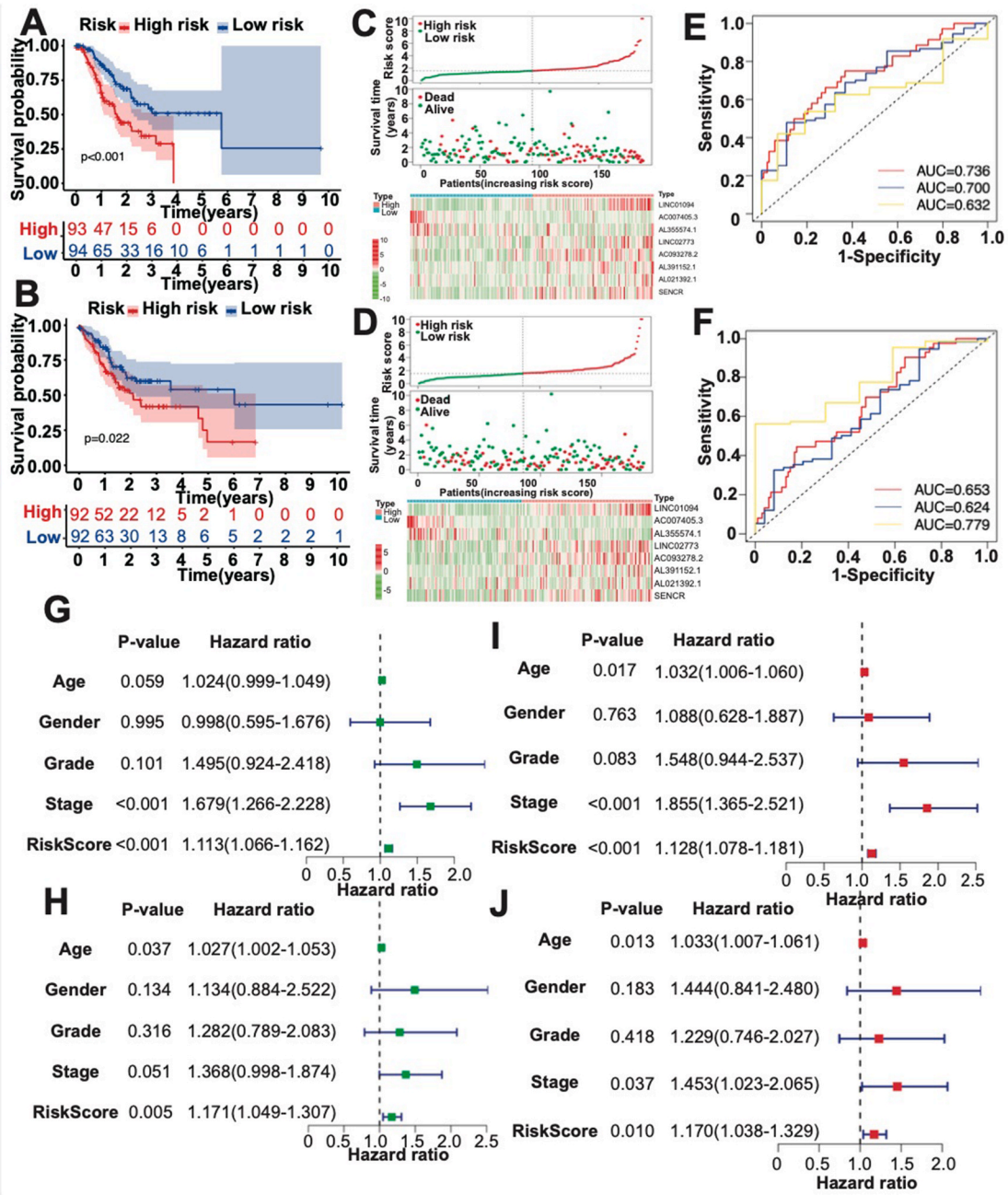

Fig. 3. The APOBEC3-related LPS predicts the OS rate of GC patients. (A) Kaplan-Meier analysis of high- and low-risk patients in the training cohort. (B) Kaplan-Meier analysis of high- and low-risk patients in the testing cohort. (C) The risk score and the death or survival of each patient in the training cohort are shown. According to the median of the risk score, the GC patients were divided into high- and low-risk groups. The expression of the APOBEC3-related LPS in each sample of the training cohort is shown in the heatmap. (D) The risk score and the death or survival of each patient in the testing cohort are shown. Additionally, the expression of the APOBEC3-related LPS in each sample of the testing cohort is shown in the heatmap. (E) ROC analysis of the APOBEC3-related LPS in the training cohort. The 1-, 3- and 5-year AUCs in the training cohort are shown. (F) ROC analysis of the APOBEC3-related LPS in the testing cohort. The 1-, 3- and 5-year AUCs in the testing cohort are shown. (G) Univariate Cox regression analysis performed on the training cohort. (H) Univariate Cox regression analysis performed on the test cohort. (I) Multivariate Cox regression analysis performed on the training cohort. (J) Multivariate Cox regression analysis performed on the testing cohort.

Low-risk patients exhibited a more favorable survival status compared to high-risk patients. We also examined the expression of the APOBEC3-related LPS in the two cohorts. The expression levels of LINC01094, LINC02773, AC093278.2, AL391152.1, AL021392.1 and SENCR were high in the high-risk group. Nevertheless, AC007405.3 and AL355574.1 were greatly expressed within the low-risk group. Here, the findings were the same in the testing as well as training cohorts (Fig. 3C and D). To estimate the accuracy of the APOBEC3-related LPS in an effort to predict 1-, 3- and 55year survival, we performed a ROC analysis and calculated the AUC. The 1-, 3- as well as 5-year AUCs were 0.736, 0.7 and 0.632, accordingly, in the training cohort. Meanwhile, in the testing cohort, the 1-, 3- as well as 5-year AUCs were 0.653, 0.624 and 0.779, correspondingly (Fig. 3E and F). The ROC analysis thus demonstrated that our APOBEC3-related LPS is accurate and sensitive.

Furthermore, we conducted multivariate and univariate Cox regression analyses in both the training and testing cohorts to explore if the APOBEC3-related LPS could act as an independent prognostic marker. According to the univariate Cox regression analysis, the risk score with regards to the APOBEC3-related LPS was linked to a low OS in both the training cohort (P value less than 0.001; hazard ratio: 1.113, 95% CI: 1.066–1.162) and the testing cohort (P-value = 0.005; hazard ratio: 1.171, 95% CI: 1.049–1.307) (Fig. 3G and H). Similarly, relying on the multivariate Cox regression analysis, the risk score was indicated to be associated to poor OS in the training cohort (P value less than 0.001; hazard ratio: 1.128, 95% CI: 1.078–1.181) and test cohort (P value = 0.01; hazard ratio: 1.17, 95% CI: 1.038–1.329) (Fig. 3I and J). In addition, we conducted a univariate Cox regression with regards to the risk score in subgroups and determined that the risk score was significant in all subgroups except subgroup Grade_G1, which could be explained by an insufficient samples size (Suppl. Fig. S2). In summary, the APOBEC3-related LPS that we constructed was identified as potential independent prognostic marker for GC patients.

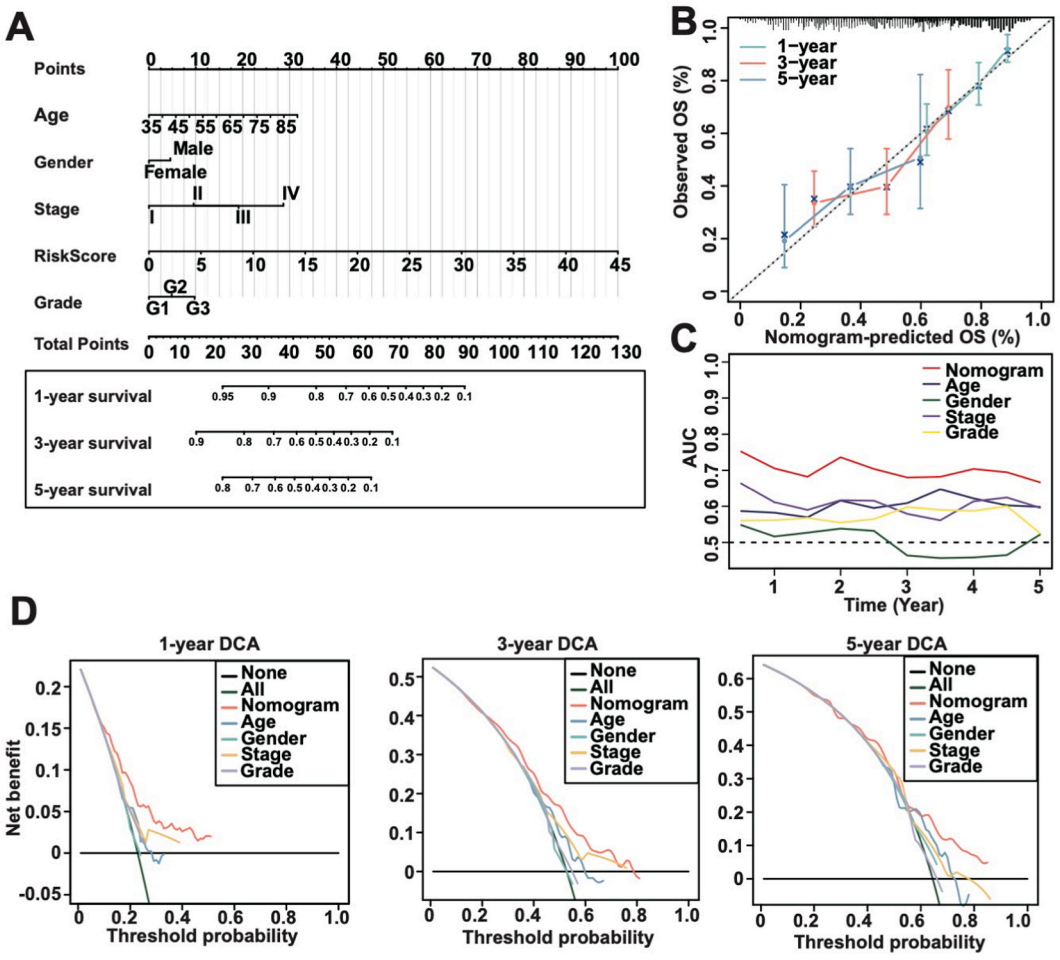

Fig. 4. Construction of a nomogram based on the APOBEC3-related LPS for GC patients. (A) A nomogram was constructed based on the risk score of the APOBEC3-related LPS. (B) The calibration curve was calculated to evaluate the stability of the nomogram in predicting 1-, 3- and 5-year survival. (C) The AUC analysis of the nomogram, testing each parameter. (D) 1-, 3- and 5-year DCA performed to compare the net clinical benefits of the nomogram.

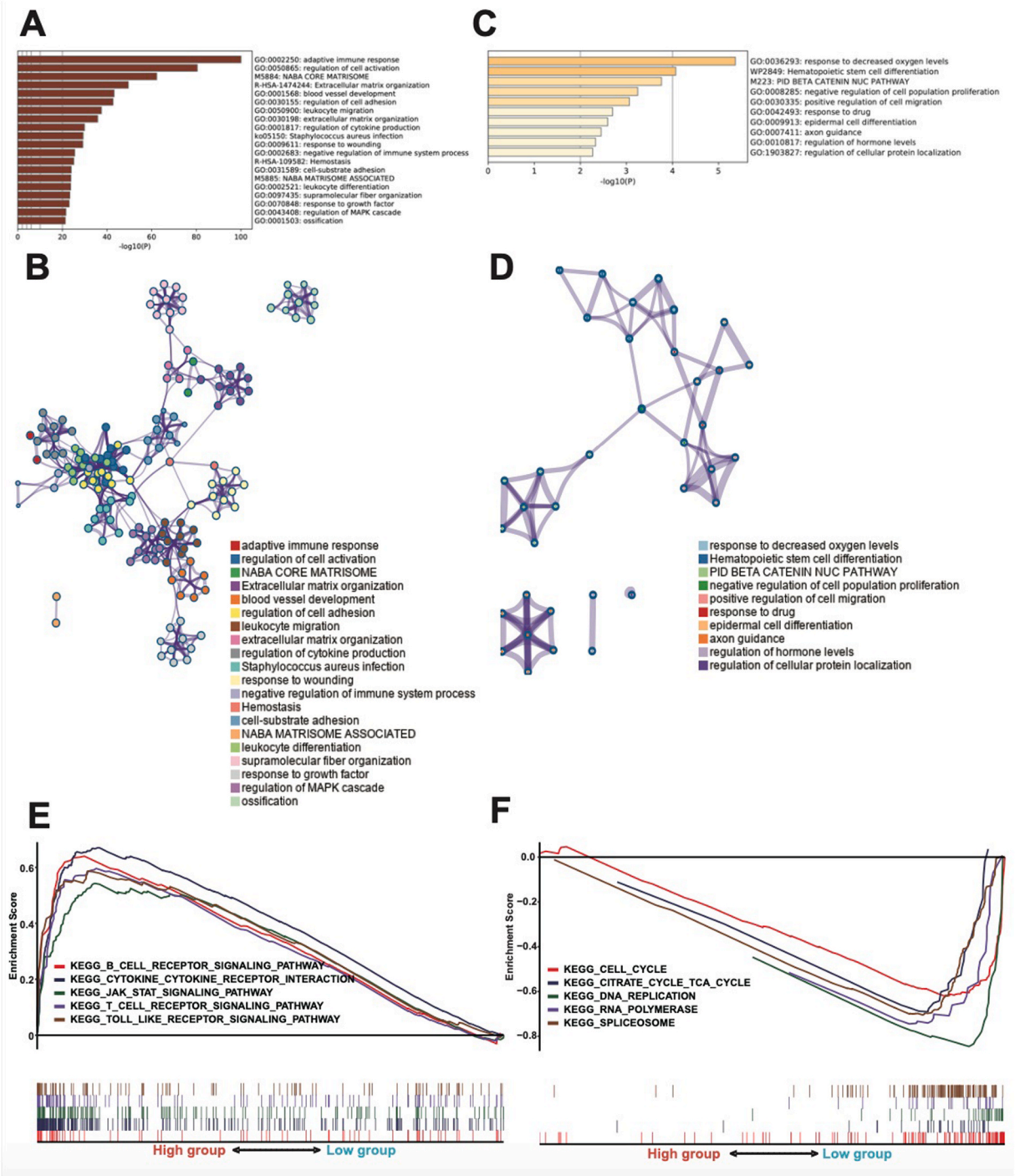

Fig. 5. Functional analysis of the APOBEC3-related LPS. (A) The online enrichment analysis tool Metascape was used after obtaining differentially expressed genes between high- and low-risk samples with the R package "limma". The significantly enriched items in high-risk samples are shown. (B) The corresponding network of enriched items in high-risk samples is shown. (C) The significantly enriched items in low-risk samples are shown using Metascape. (D) The corresponding network of enriched items in low-risk samples is shown. (E) GSEA was performed, and the pathways enriched in high-risk samples are shown. (F) The pathways enriched in low-risk samples are shown.

4.4. APOBEC3-related LPS is a suitable nomogram prognostic prediction factor

To better identify the prognostic value with regards to the APOBEC3-related LPS, we constitute a nomogram relying on the risk score of the APOBEC3-related LPS (Fig. 4A). Points were allocated to each parameter on the axes of individual point scale. The cumulative points can be obtained by summing the individual points. Afterward, the cumulative points can be projected onto the lower survival scales, allowing us to foresee the 1-, 3- as well as 5-year OS rates. As an example, a 65-year-old (17.5 points) male (5 points) patient with stage III GC (18.5 points), a G2 tumor grade (5 points) and a risk score of 10 (22 points) received a cumulative of 68 points, which means that the patient's predicted 1-, 3- as well as 5- year survival rates were approximated to be 48%, 10% and less than 10%, respectively.

We constructed a calibration curve (Fig. 4B) to assess our nomogram. Moreover, the calibration curves for the 1-, 3- as well as 5-year survival rates were essentially similar. Moreover, we conducted a time-dependent ROC analysis (Fig. 4C) and found that the nomogram we constructed displayed the greatest AUC in comparison to a single parameter, which indicated that our nomogram's prediction accuracy was better than that of each individual parameter. Ultimately, we conducted a DCA to estimate if the nomogram was useful. The 1-, 3- as well as 5-year DCA indicated that the net benefit with regards to our nomogram model was greater compared to that of each individual parameter (Fig. 4D). Overall, we concluded that the constructed nomogram had higher prognostic value than utilizing a single individual parameter in predicting the prognosis concerning GC patients.

4.5. Enrichment analysis of the APOBEC3-related LPS

Matascape. an online enrichment analysis tool, was used for investigating the function of the APOBEC3-related LPS. After obtaining the differentially expressed genes among high-as well as low-risk patients, we input the gene set into Metascape; the significantly enriched terms in the high-risk group as well as the corresponding network are shown (Fig. 5A and B) (Table S1). The five significantly

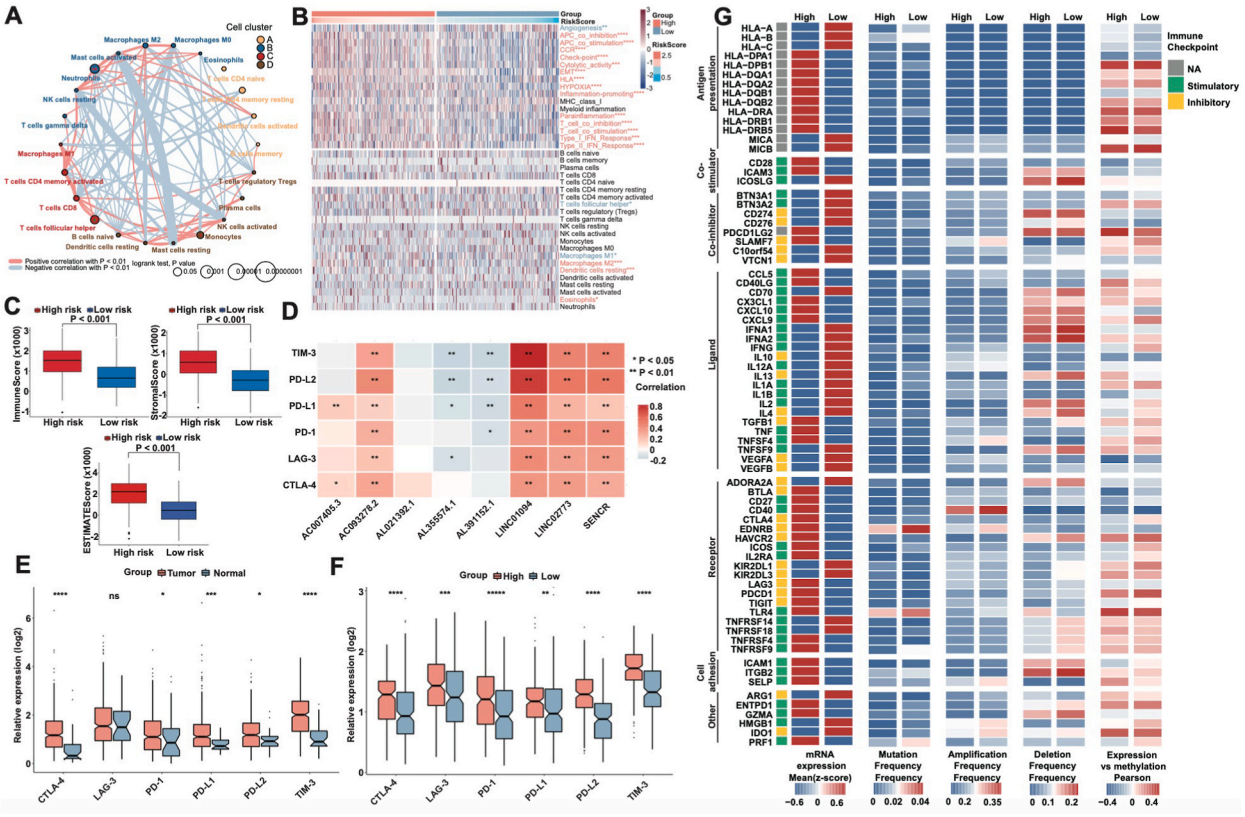

Fig. 6. Immune analysis of the APOBEC3-related LPS. (A) The network of correlations of 22 TICs and the significant prognostic TICs is shown. *red: HR > 1; *green: HR < 1. (B) The enrichment status of pathways of interest and the expression of 22 TICs are shown in the heatmap. Red represents the pathways that were enriched in the high-risk group, and blue represents the pathways that were enriched in the low-risk group. (C) The immune, stromal and ESTIMATE scores were calculated in high- and low-risk patients. (D) The correlation of the six immune checkpoints and the APOBEC3-related LPS. (E) The relative expression of the six immune checkpoints in GC and normal tissue is shown. (F) The relative expression of the six immune checkpoints in high- and low-risk patients is shown. ns: not statistically significant. (G) Mutiomics analysis of 75 immunomodulators in high- and low-risk patients with GC. *P < 0.05, **P < 0.01, ***P < 0.001. (For interpretation of the references to colour in this figure legend, the reader is referred to the Web version of this article.)

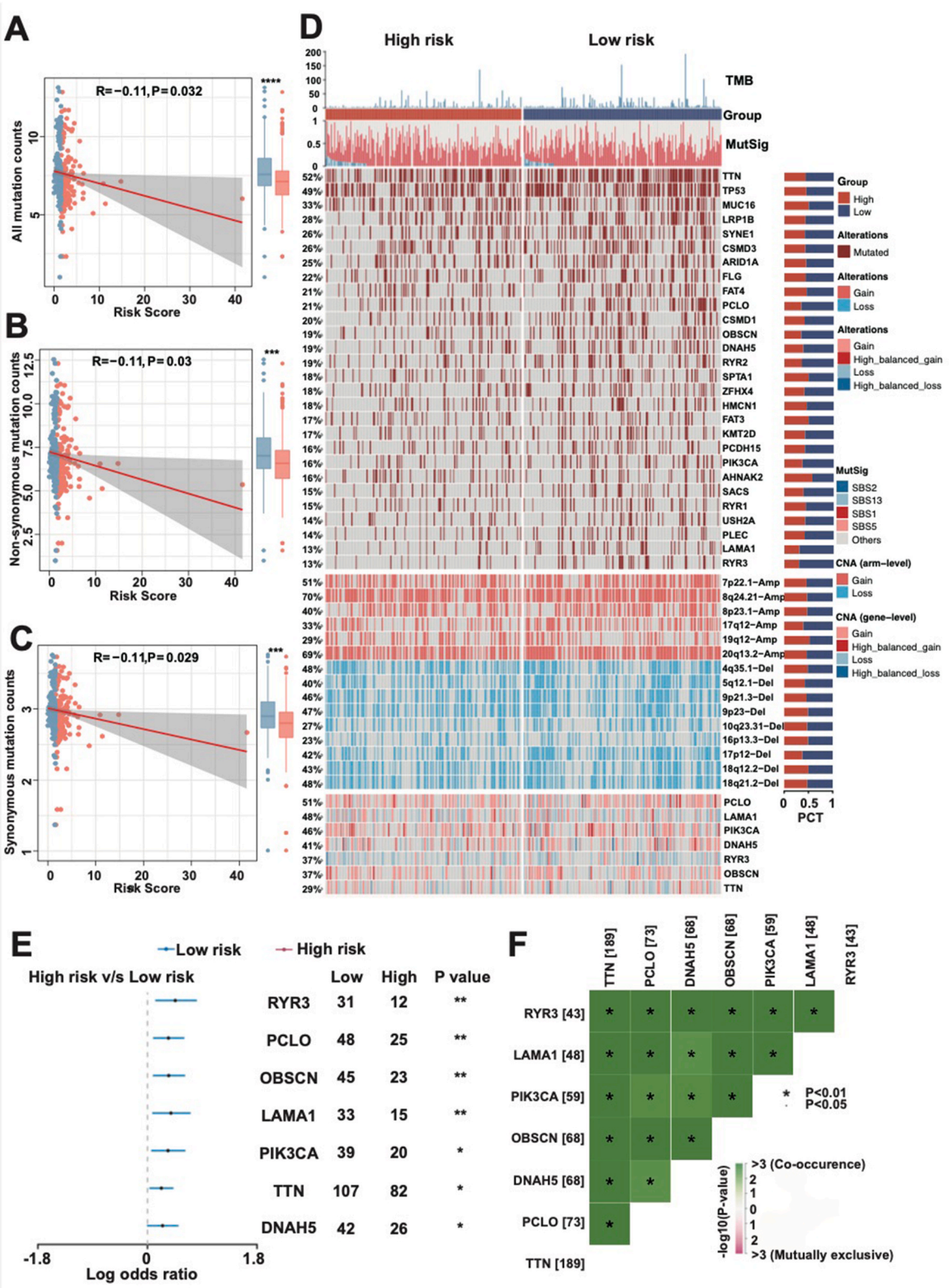

Fig. 7. Mutation analysis of the APOBEC3-related LPS. (A) All mutation counts were detected in each sample. The red bar represents the mutation counts in the high-risk patients, while the blue bar represents the mutation counts in the low-risk patients. (B) Nonsynonymous mutation counts in each sample. (C) Synonymous mutation counts in each sample. (D) The mutational landscapes in high- and low-risk samples is shown. The TMB and MutSig spectra of each sample were evaluated. Genes with minimum mutation counts greater than 30 are shown. The percentage of

amplifications and deletions of genes were evaluated by CNA analysis. (E) The significantly mutated genes in high- and low-risk patients are shown in the forest plot. (F) The co-occurrence and mutual exclusivity analyses of the seven genes are shown. *P < 0.05, **P < 0.01, ***P < 0.001. (For interpretation of the references to colour in this figure legend, the reader is referred to the Web version of this article.)

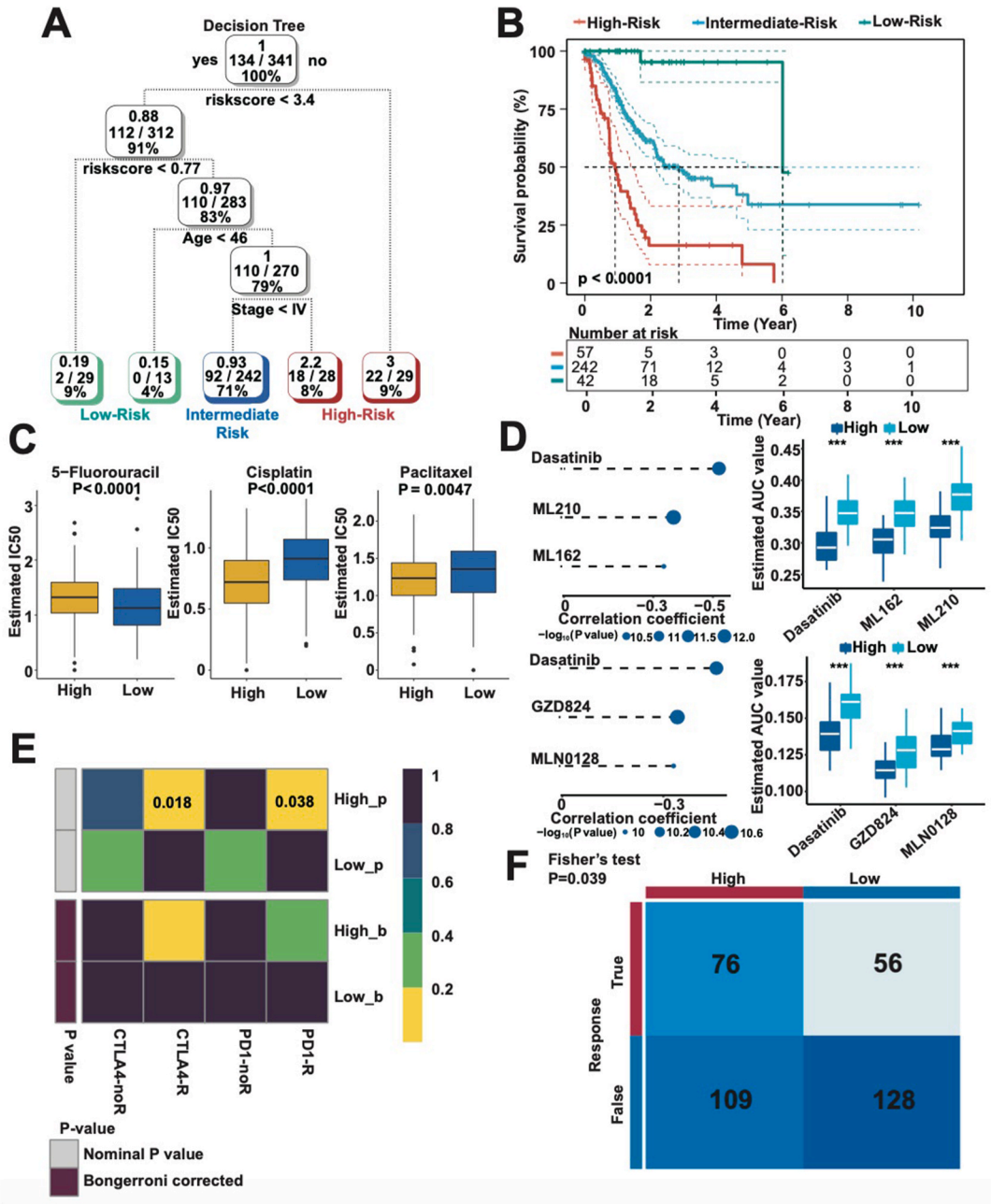

Fig. 8. The APOBEC3-related LPS guides the clinical treatment. (A) A decision tree was constructed based on the risk score, age and stage of GC patients using the "rpart" R package in R studio. GC patients were divided into low-risk, intermediate-risk and high-risk subgroups. (B) Kaplan-Meier analysis was performed to detect the OS rate of the three subgroups. (C) Three common drugs for treating GC were selected and their estimated IC50 in high- and low-risk patients was analyzed based on the GDSC database. (D) The predicted drug sensitivity is shown. The CTRP 2.0 and PRISM databases were used to predict the potential sensitivity of small-molecule drugs. The correlation coefficients between drugs and high-risk score as well as the estimated AUC value were calculated. (E) Detected immune responses to PD-1 and CTLA4. (F) Total immune response was evaluated using Fisher's test.

enriched items ranked at the top were adaptive immune response, regulation of cell activation, NABA CORE MATRISOME, extracellular matrix organization and blood vessel development. Additionally, the significantly enriched terms in the low-risk group are also displayed in a bar graph (Fig. 5C) (Table S2), and the corresponding network is depicted (Fig. 5D). As for the low-risk group, responses to decreased oxygen levels, hematopoietic stem cell differentiation, PID BETA CATENIN NUC PATHWAY, negative regulation of cell population proliferation as well as positive regulation with regards to cell migration were the top five enriched items. Then, we conducted GSEA to detect the pathways enriched in high-risk or low-risk patients. We discovered that B and T cell receptor signaling, JAK-STAT signaling, cytokine-cytokine receptor interaction as well as Toll-like receptor signaling pathways were significantly enriched in the high-risk group (Fig. 5E) (Table S3). The DNA replication, cell cycle, citrate cycle TCA cycle, RNA polymerase as well as spliceosome were enriched in the low-risk patients (Fig. 5F) (Table S4).

4.6. Immune analysis of the APOBEC3-related LPS

The 22 TICs were separated into four subgroups according to hierarchical cluster analysis. Correlations among the TICs were determined, and the univariate Cox regression analysis of the TICs was conducted. The findings indicated that activated mast cells exhibited a markedly negative correlation with resting mast cells and that follicular helper T cells were related to better OS. However, neutrophils and monocytes were associated with lower OS (Fig. 6A). Furthermore, we examined pathways of interest via ssGSEA and demonstrated that the samples accompanied by high-risk scores were positively associated with certain pathways, such as the checkpoint, EMT, hypoxia, and inflammation pathways. The samples accompanied by high-risk scores were also enriched in T cells and type I as well as II activation. The only pathway that was enriched in the low-risk group was angiogenesis. Furthermore, we also measured the relative abundance of the 22 TICs in each sample. M1 macrophages as well as Follicular helper T cells were greatly expressed in low-risk patients. However, the abundance of resting dendritic cells, eosinophils and M2 macrophages was upregulated in high-risk patients (Fig. 6B). Afterward, we performed a TME analysis. The stromal, ESTIMATE and immune scores were all greater in high-risk patients in comparison to low-risk patients (P less than 0.001) (Fig. 6C).

Since immune checkpoints have been found to control immune homeostasis by inducing cancer cells to evade immune attacks [28], we were curious about the connection between the APOBEC3-related LPS with immune checkpoints. Thus, we analyzed the correlation among six common immune checkpoints (which includes TIM-3, PD-L2, PD-L1, PD-1, LAG-3 as well as CTLA-4) and the APOBEC3-related LPS (Fig. 6D). We found that AC093278.2, LINC01094, LINC02773 and SENCR were all significantly positively correlated with the six checkpoints. AC007405.3 was positively associated with PD-L1 as well as CTLA-4. AL355574.1 had a negative correlation with TIM-3, PD-L2, PD-L1 and LAG-3. AL391152.1 was negatively correlated with TIM-3, PD-L2, PD-L1 and PD-1. Nevertheless, we did not observe any significant relationship among AL021392.1 and the six checkpoints. Afterward, we evaluated the relative expression of the six checkpoints in the GC and normal samples. We observed that, except for LAG-3, all checkpoints were upregulated in the GC samples in comparison to normal samples (Fig. 6E). Lastly, we assessed the relative expression with regards to the six checkpoints in the high-as well as low-risk groups. Interestingly, all the checkpoints were greatly expressed in the high-risk group in contrast to the low-risk group (Fig. 6F). Then, we performed a multiomics analysis of 75 immunomodulators (including antigen presentation factors, costimulators, coinhibitors, ligands, receptors, and cell adhesion factors) among high-as well as low-risk GC patients (Fig. 6G). The findings depicted variations in mutation frequency, mRNA expression, amplification and deletion frequency, including gene expression correlation with the DNA methylation beta value among high-as well as low-risk patients.

4.7. Patients with a high-risk according to APOBEC3-related LPS have a lower rate of mutation

We were curious with regard to the mutation status in high-as well as low-risk GC patients. Therefore, we measured the mutation counts of all samples and discovered that patients with low risk exhibited a greater mutation count. Moreover, based on Pearson's correlation analysis, all mutation counts and risk scores were significantly negatively correlated (R value = −0.11 and P value = 0.032) (Fig. 7A). Moreover, we also counted nonsynonymous mutations as well as synonymous mutations. Both nonsynonymous and synonymous mutation counts were higher in low-risk GC patients and were negatively correlated with risk scores (R value = −0.01, P value = 0.03 and 0.029, respectively) (Fig. 7B and C). Then, we constructed a mutational landscape in order to perform analysis of the mutational differences among high-as well as low-risk samples (Fig. 7D). We screened for genes in which the minimum mutation counts were more than 30. We also conducted a CNA analysis to determine the amplifications and deletions of each sample. As we expected, more mutations were found in low-risk GC patients. The forest plot revealed seven genes (RYR3, PCLO, OBSCN, LAMA1, PIK3CA, TTN and DNAH5) that were greatly expressed in low-risk patients (Fig. 7E). Then, the percentage of CNAs of the seven genes was determined in each sample (Fig. 7D). In addition, we performed mutual exclusivity as well as co-occurrence analysis of the seven genes (Fig. 7F), which revealed that the mutations of the seven genes tend to co-occur.

4.8. The APOBEC3-related LPS guides the clinical treatment decisions in GC

Relying on the risk score, age as well as tumor stage of the GC patients, we created a decision tree to separate patients into three subgroups: low-risk, intermediate-risk as well as high-risk groups. The pivotal factor was the risk score, which had the most weight in our decision tree (Fig. 8A). Through this decision tree, we discovered that 71% of GC patients were in the intermediate-risk subgroup, which means that the majority of GC patients had a risk score from 0.77 to 3.4, were more than 46 years old, and were below stage IV. Additionally, we performed a Kaplan-Meier analysis to explore the survival among the three subgroups (Fig. 8B). The patients in the high-risk subgroup exhibited the lowest rate of survival. The low-risk patients had the best survival rates among the three subgroups.

The main treatment for GC patients is 5-fluorouracil-based chemotherapy; therefore, we made a prediction regarding the drug sensitivity of the three primary chemotherapeutic drugs for high- and low-risk patients, which were classified relying on the risk score including the expression of the APOBEC3-related LPS (Fig. 8C). The sensitivity of 5-fluorouracil was higher in low-risk patients. Nonetheless, the sensitivities of cisplatin and paclitaxel were higher in high-risk patients. Since 5-fluorouracil possessed lower sensitivity in high-risk patients, we predicted several small-molecule drugs that exhibited greater sensitivity in high-risk patients using two different methods (Fig. 8D). We found that the predicted small-molecule drugs displayed a negative correlation with the risk score as well as exhibited a minimized estimated AUC value in high-risk patients, which indicated that these small-molecule drugs had greater sensitivity in high-risk GC patients. Of these drugs, dasatinib was significant in both methods and might be considered a potential novel drug for treating high-risk GC patients. Next, we utilized subclass mapping in predicting the immune response to the immune checkpoint blockades PD1 as well as CTLA4 in GC patients (Fig. 8E). The responses to PD-1 as well as CTLA4 were significant in high-risk patients (P value = 0.038 and 0.018, correspondingly). Furthermore, the TIDE algorithm assessed the total immune response between high-as well as low-risk patients, which discovered that the high-risk patients exhibited an enhanced immune response (P = 0.039)(Fig. 8F). Finally, we performed MoA analysis to predict the possible drugs for GC treatment and their corresponding mechanisms (Suppl. Fig. S3).

4.9. Effects of LINC01094 overexpression on cell proliferation, migration, apoptosis, and macrophage polarization in KATO cells and GES-1 cells

Because LINC01094 is the most powerful risk factor in the named LINC RNA. Therefore, we chose LINC01094 for further validation. We determined the expression of LINC01094 by QT-qPCR after overexpression of KATO-2 cells (Fig. 9A). In comparison to the control group, the expression with regards to LINC01094 was substantially upregulated after KATO-2 transfection. Subsequently, we examined the impacts of LINC01094 overexpression on the migration as well as proliferation of gastric cancer cell lines. As shown in Fig. 9B, the EDU staining of KATO cells was even more pronounced after LINC01094 overexpression. Meanwhile, CCK-8 also demonstrated greater proliferative cells (Fig. 9C). Meanwhile, we examined the migratory ability of the cells. As shown in Fig. 9D and E, after LINC01094 overexpression, the cells migrated faster than the normal KATO cells. Moreover, Tunel staining for cell apoptosis indicated that the apoptosis of tumor cells was inhibited after LINC01094 overexpression (Fig. 9F and G). This indicates that this indicates that LINC01094 can enhance KATO-2 migration and proliferation in tumor cells. Finally, to verify that APOBEC3-associated LPS is associated with changes in the immune microenvironment, we stained macrophages. The findings of the experiment are shown in Fig. 9H and I, after overexpression of LINC01094, macrophages were polarized to M2 and the expression of M2 marker CD206 was increased.

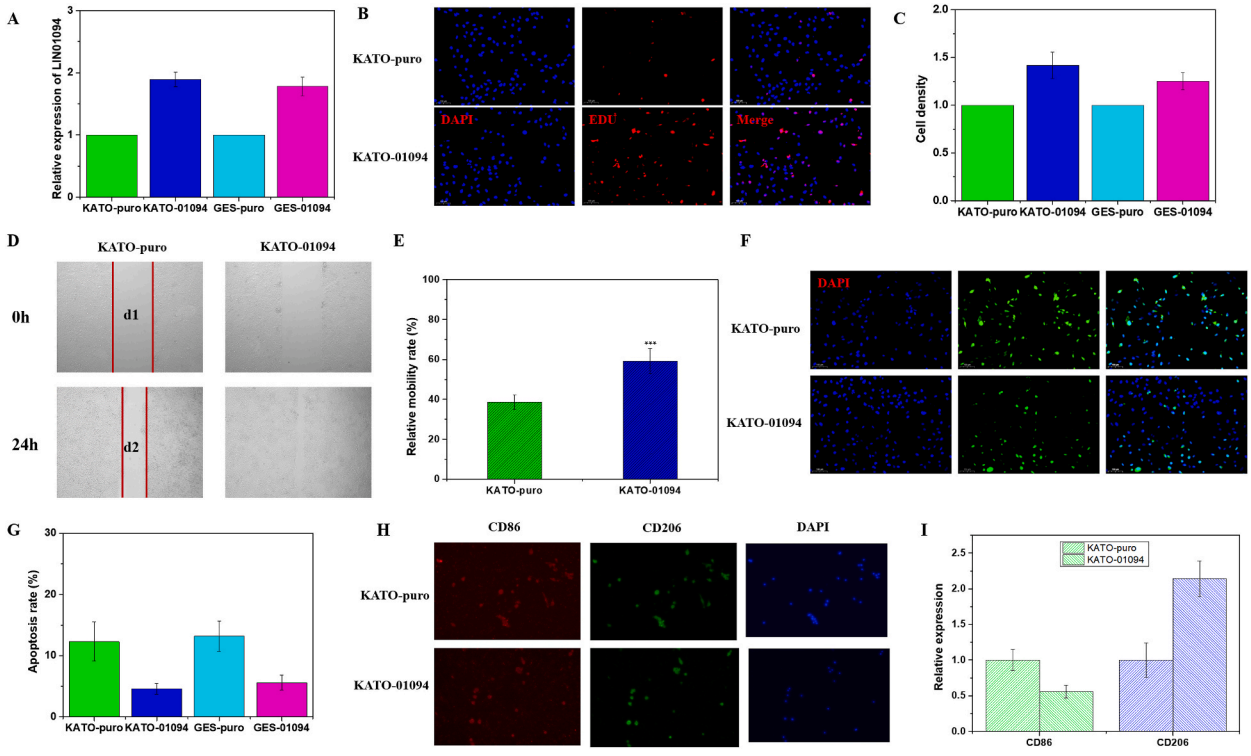

Fig. 9. Effects of LINC01094 overexpression on cell proliferation, migration, and apoptosis in KATO cells and GES-1 cells. (A) QT-qPCR to detect the relative expression of LINC01094. (B) EDU assay of KATO cells overexpressing LINC01094 and normally expressing LINC01094. (C)CCK-8 cell proliferation assay. (D and E) Cell migration; Tunel staining for apoptosis(F and G), and macrophage polarization (H and I). ***P < 0.0001.

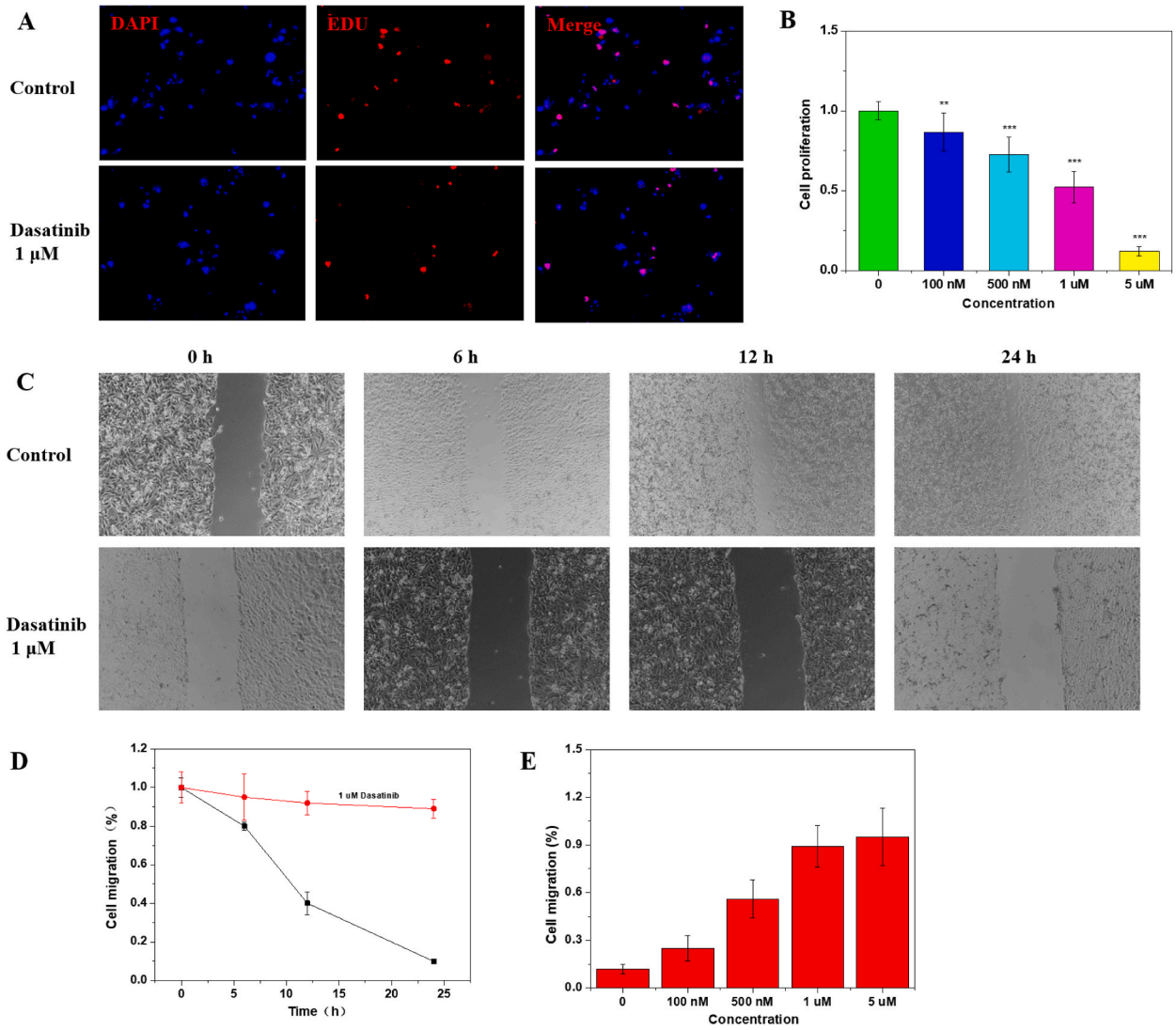

Fig. 10. Inhibitory effect of Dasatinib on the proliferation and migration of KATO cells. (A) Typical pictures of KATO cells treated with different concentrations of Dasatinib. (B) Statistical analysis of KATO cells treated with different concentrations of Dasatinib. (C) Typical pictures of 1 μM Dasatinib treated KATO cells at different time points. (D) Quantitative analysis of 1 μM Dasatinib treated KATO cells at different time points. (E) Statistical analysis of KATO cells treated with different concentrations of Dasatinib.

4.10. The inhibitory effect of dasatinib on the proliferation and migration of KATO cells

Dasatinib is a potent anticancer drug that can exert an antitumor effect by impeding the growth along with spread of tumor cells. Next, we also verified whether our predicted drugs were effective by co-culture of Dasatinib with KATO cells. As illustrated in Fig. 10A as well as B, Dasatinib effectively impeded the gastric cancer cells proliferation, as well as the inhibitory effect increased with increasing Dasatinib concentration. Meanwhile, we also analyzed the effect of Dasatinib on gastric cancer cell migration, as shown in Fig. 10C and D, the migration of KATO of GC cells was inhibited with increasing concentration and time extension(Fig. 10E). This indicates that the drugs we predicted could indeed inhibit the increase and migration of GC cells. This may be related to the remodeling of the cytoskeleton and requires further experimental inflammation.

5. Discussion

GC refers to the most prevalent malignancy in the gastrointestinal system, with a substantial rate of recurrence and a low 5-year OS rate [29]. Therefore, it is vital to predict patient prognosis and discover possible novel drugs for treating GC. LncRNAs have recently been verified to be linked with the development of cancer as well as act as cancer biomarkers [30]. In addition, many studies have revealed that the APOBEC3 family genes are related to immunity and linked to cancer development [31]. According to our previous

research, APOBEC3G is closely related to lncRNA H19 [16]. Hence, we were curious whether it was possible to develop a prognostic signature according to APOBEC3-related lncRNAs.

In the current research, we first established a promising individual APOBEC3-related LPS and then evaluated this APOBEC3-related LPS thoroughly, including clinical, functional, immune, and mutation analyses as well as its role in therapy decisions. According to our analysis, our constructed LPS was involved in many pathways. The APOBEC3-related LPS was strongly correlated with the immune system. Thus, we analyzed typical immune checkpoints and found a strong correlation between them and the APOBEC3-related LPS. Seven mutated genes, which might be regarded as the triggers of GC development, were uncovered based on the APOBEC3-related LPS. In the clinic, the APOBEC3-related LPS could be considered a clinical tool to predict GC patient prognoses and select possible treatments.

We determined differentially expressed genes among high-as well as low-risk samples and explored the enriched function of the APOBEC3-related LPS. Thanks to Metascape, we easily obtained significantly up-and downregulated items. As expected, the adaptive immune response was the most significantly upregulated enriched function, thus demonstrating that the APOBEC3-related LPS was strongly correlated with immunity. In addition, the GSEA indicated that the B/T cell receptor signaling pathway was significantly enriched in high-risk samples, affirming the close relationship among immunity and the APOBEC3-related LPS. We also observed that several cancer-related pathways were enriched, like cytokine receptor as well as cytokine interaction [32], the JAK/STAT signaling pathway [33], cell cycle [34], TCA cycle [35], DNA replication [36] as well as the Toll-like receptor signaling pathway [37], which suggested that the APOBEC3-related LPS might participate in the regulation of cancer progression.

Since the functional analysis confirmed that the APOBEC3-related LPS was associated with the immune system, we were interested in further investigating this relationship. First, we performed a cluster analysis to divide 22 TICs into four subgroups in GC according to their correlation. By performing univariate Cox regression analysis according to the risk score, we observed that neutrophils and monocytes predicted worse OS, while follicular helper T cells were associated with the better OS. Our results aligned with those of previous articles: one that reported that tumor-activated neutrophils fostered cancer progression and reduced the survival of GC patients [38], one that revealed that monocyte count was a negative prognostic factor [39], and another that reported that follicular helper T cells predicted clinical prognosis in lung squamous cell carcinoma [40]. According to the risk score assessed from the APOBEC3-related LPS, we discovered that immune-related and cancer-related pathways were enriched in the high-risk group. This proposed that GC patients with high risk had greater active immune and cancer development regulation. Moreover, M1 macrophages were expressed in high-risk patients at lower levels, while M2 macrophages were expressed at higher levels. This result was consistent with prior research that suggested that macrophages in tumors were biased toward M2 macrophage rather than M1 macrophage [41]. Immune checkpoints function as an brake to inhibit T cell overreaction but are used by tumor cells to evade immune surveillance [42]. The close correlation between immune checkpoints and the APOBEC3-related LPS suggests that the eight lncRNAs might be involved in immune escape in GC. Moreover, the expression of immune checkpoints was upregulated not only in GC but also in high-risk patients, which may suggest stronger immunogenicity and better immune therapy sensitivity in high-risk patients.

By comparing the mutation counts of high-as well as low-risk patients, we discovered that seven genes were significantly mutated in low-risk patients. Most of these genes are considered to be cancer promoters. For instance, ryanodine receptor 3 (RYR3) has been proven in regulating growth and migration in breast cancer [43]. TRA2B-DNAH5 fusion has been determined to be novel oncogenic driver [44]. PIK3CA functions as an oncogene, resulting in uncontrolled cell proliferation, growth and tumorigenesis [45], and patients with PIK3CA-mutated triple-negative breast cancer exhibit a favorable OS [46]. Knockdown of PCLO expression decreased the esophageal squamous cell carcinoma malignancy both *in vitro* and *in vivo* [47]. LAMA1 has been identified to be significantly upregulated in esophageal squamous cell carcinoma tissues and is positively correlated with the aggressive oncogenic phenotype. The circPDE3B/miR-4766-5p/LAMA1 axis operates as an oncogenic factor to promote cell proliferation, invasion and migration [48]. Therefore, more frequent mutations of these genes in low-risk patients suggests that the function of theses oncogenes were attenuated.

A nomogram was establsihed for predicting the individual GC patients prognosis relying on the risk score of the APOBEC3-related LPS. The accuracy as well as superiority of our nomogram were quantified using calibration curve, AUC and DCA analyses [49]. The results demonstrate that our constructed nomogram has an adequate predictive value. Moreover, we further considered how our constructed APOBEC3-related LPS could guide our clinical treatment. We used it to predict drugs that might exhibit higher sensitivity in high-risk patients. Dasatinib was predicted to improved sensitivity in high-risk patients by two methods. Recently, dasatinib has been proven to be an inhibitor of GC proliferation *in vitro* [50]. The synergistic antitumor effects of oxaliplatin and dasatinib in GC were found *in vivo* and *in vitro* [51]. In the current research, it was also confirmed that Dasatinib did inhibit the migration and proliferation with regards to KATO cells in gastric cancer cells.Therefore, dasatinib might be considered a potential drug for GC patients.

Although we successfully constructed an APOBEC3-related LPS and thoroughly analyzed its predictive value, our study had several constraints. Firstly, our data originated from public databases. Although the necessary analyses were performed to verify the predictive power of the APOBEC3-related LPS, the real-world clinical cohorts ought to be involved in certifying our results. Second, we have not performed experiments to prove our results; Thus, the functions and mechanisms of the APOBEC3-related LPS in GC need to be further verified *in vitro* and *in vivo*. Third, the constructed APOBEC3-related LPS should be subjected to prospective validation before clinical applications.

LINCRNA is a key regulator involved in various cancer progression. LINC01094 is frequently upregulated in renal cell carcinoma as well as gliomas. Research have found that elevated LINC01094 expression predicts weak gastric cancer prognosis and is associated with the epithelial-mesenchymal transition pathway as well as macrophage infiltration [52]. Nevertheless, its function in GC remains ambiguous. Our research found an important function of LINC01094 in GC. By experimental validation, we found that LINC01094 expression was significantly upregulated in KATO-2. Further studies showed that overexpression of LINC01094 could promote migration and proliferation with regards to gastric cancer cells while inhibiting apoptosis. Moreover, we founded that LINC01094

overexpression causes macrophage polarization on the M2 type as well as increased expression of the M2 marker CD206. These results suggested that LINC01094 has a promoting function in the GC development as well as may serve as a promising therapeutic biomarker. Meanwhile, we also found that APOBEC3 is associated with LINC01094, which could further scrutinize the function of LINC01094 in the immune microenvironment.

To summarize, the APOBEC3-related LPS was linked with immune- and cancer-related pathways and was an accurate and superior tool to individually predict GC patient prognosis. Furthermore, the APOBEC3-related LPS might be a guide for clinical treatment and predict patient immune response.

Consent for publication

All authors concur regarding the publication of this manuscript. This work has not been published previously and is not presently under the consideration for publication elsewhere.

Funding

This work was supported in part by the Medical Science and Technology Project of Zhejiang Province (Grant No. WKJ-ZJ-2310). The funders had no role in the study design, data collection, analysis, publication decision, or manuscript preparation.

CRediT authorship contribution statement

Jia Qi: Writing – original draft. **Wenxuan Wu:** Writing – original draft. **Jing Chen:** Data curation. **Xiaying Han:** Data curation. **Zhixing Hao:** Formal analysis. **Yaxuan Han:** Methodology. **Yewei Xu:** Validation. **Jun Lai:** Writing – review & editing. **Jian Chen:** Writing – review & editing.

Declaration of competing interest

The authors declare that they have no known competing financial interests or personal relationships that could have appeared to influence the work reported in this paper.

Appendix A. Supplementary data

Supplementary data to this article can be found online at https://doi.org/10.1016/j.heliyon.2024.e28307.

References

[1] E.C. Smyth, M. Nilsson, H.I. Grabsch, N.C. van Grieken, F. Lordick, Gastric cancer, Lancet (London, England) 396 (10251) (2020) 635–648.
[2] R. De Angelis, M. Sant, M.P. Coleman, S. Francisci, P. Baili, D. Pierannunzio, et al., Cancer survival in Europe 1999-2007 by country and age: results of EUROCARE–5-a population-based study, Lancet Oncol. 15 (1) (2014) 23–34.
[3] F. Lordick, K. Shitara, Y.Y. Janjigian, New agents on the horizon in gastric cancer, Ann. Oncol. : Off. J. Eur. Soc. Med. Oncol. 28 (8) (2017) 1767–1775.
[4] A. Jarmuz, A. Chester, J. Bayliss, J. Gisbourne, I. Dunham, J. Scott, et al., An anthropoid-specific locus of orphan C to U RNA-editing enzymes on chromosome 22, Genomics 79 (3) (2002) 285–296.
[5] S. Revathidevi, A.K. Murugan, H. Nakaoka, I. Inoue, A.K. Munirajan, APOBEC: a molecular driver in cervical cancer pathogenesis, Cancer Lett. 496 (2021) 104–116.
[6] D. Xuan, G. Li, Q. Cai, S. Deming-Halverson, M.J. Shrubsole, X.O. Shu, et al., APOBEC3 deletion polymorphism is associated with breast cancer risk among women of European ancestry, Carcinogenesis 34 (10) (2013) 2240–2243.
[7] C.D. Middlebrooks, A.R. Banday, K. Matsuda, K.I. Udquim, O.O. Onabajo, A. Paquin, et al., Association of germline variants in the APOBEC3 region with cancer risk and enrichment with APOBEC-signature mutations in tumors, Nat. Genet. 48 (11) (2016) 1330–1338.
[8] G. Qi, H. Xiong, C. Zhou, APOBEC3 deletion polymorphism is associated with epithelial ovarian cancer risk among Chinese women, Tumour biology : the journal of the International Society for Oncodevelopmental Biology and Medicine 35 (6) (2014) 5723–5726.
[9] J.D. Salter, R.P. Bennett, H.C. Smith, The APOBEC protein family: united by structure, divergent in function, Trends Biochem. Sci. 41 (7) (2016) 578–594.
[10] S. Zhang, C. Qin, G. Cao, W. Xin, C. Feng, W. Zhang, Systematic analysis of long noncoding RNAs in the senescence-accelerated mouse prone 8 brain using RNA sequencing, Mol. Ther. Nucleic Acids 5 (8) (2016) e343.
[11] A. Bhan, S.S. Mandal, LncRNA HOTAIR: a master regulator of chromatin dynamics and cancer, Biochim. Biophys. Acta 1856 (1) (2015) 151–164.
[12] A. Bhan, S.S. Mandal, Long noncoding RNAs: emerging stars in gene regulation, epigenetics and human disease, ChemMedChem 9 (9) (2014) 1932–1956.
[13] B. Goyal, S.R.M. Yadav, N. Awasthee, S. Gupta, A.B. Kunnumakkara, S.C. Gupta, Diagnostic, prognostic, and therapeutic significance of long non-coding RNA MALAT1 in cancer, Biochim. Biophys. Acta Rev. Canc 1875 (2) (2021) 188502.
[14] M. Sarfi, M. Abbastabar, E. Khalili, Long noncoding RNAs biomarker-based cancer assessment, J. Cell. Physiol. 234 (10) (2019) 16971–16986.
[15] G. Wang, Z.J. Zhang, W.G. Jian, P.H. Liu, W. Xue, T.D. Wang, et al., Novel long noncoding RNA OTUD6B-AS1 indicates poor prognosis and inhibits clear cell renal cell carcinoma proliferation via the Wnt/β-catenin signaling pathway, Mol. Cancer 18 (1) (2019) 15.
[16] Y. Luo, B. Yan, L. Liu, L. Yin, H. Ji, X. An, et al., Sulforaphane inhibits the expression of long noncoding RNA H19 and its target APOBEC3G and thereby pancreatic cancer progression, Cancers 13 (4) (2021).
[17] J.Y. Liang, D.S. Wang, H.C. Lin, X.X. Chen, H. Yang, Y. Zheng, et al., A novel ferroptosis-related gene signature for overall survival prediction in patients with hepatocellular carcinoma, Int. J. Biol. Sci. 16 (13) (2020) 2430–2441.
[18] D.F. McDermott, M.A. Huseni, M.B. Atkins, R.J. Motzer, B.I. Rini, B. Escudier, et al., Clinical activity and molecular correlates of response to atezolizumab alone or in combination with bevacizumab versus sunitinib in renal cell carcinoma, Nat. Med. 24 (6) (2018) 749–757.

[19] D.L. Gibbons, C.J. Creighton, Pan-cancer survey of epithelial-mesenchymal transition markers across the Cancer Genome Atlas, Dev. Dynam. 247 (3) (2018) 555–564.
[20] A. Liberzon, A. Subramanian, R. Pinchback, H. Thorvaldsdóttir, P. Tamayo, J.P. Mesirov, Molecular signatures database (MSigDB) 3.0, Bioinformatics 27 (12) (2011) 1739–1740.
[21] P. Jiang, S. Gu, D. Pan, J. Fu, A. Sahu, X. Hu, et al., Signatures of T cell dysfunction and exclusion predict cancer immunotherapy response, Nat. Med. 24 (10) (2018) 1550–1558.
[22] Z. Liu, L. Liu, D. Jiao, C. Guo, L. Wang, Z. Li, et al., Association of RYR2 mutation with tumor mutation burden, prognosis, and antitumor immunity in patients with esophageal adenocarcinoma, Front. Genet. 12 (2021) 669694.
[23] Z. Liu, T. Lu, L. Wang, L. Liu, L. Li, X. Han, Comprehensive molecular analyses of a novel mutational signature classification system with regard to prognosis, genomic alterations, and immune landscape in glioma, Front. Mol. Biosci. 8 (2021) 682084.
[24] Z. Liu, T. Lu, J. Li, L. Wang, K. Xu, Q. Dang, et al., Clinical significance and inflammatory landscape of aNovel recurrence-associated immune signature in stage II/III colorectal cancer, Front. Immunol. 12 (2021) 702594.
[25] Z. Liu, S. Weng, H. Xu, L. Wang, L. Liu, Y. Zhang, et al., Computational recognition and clinical verification of TGF-β-derived miRNA signature with potential implications in prognosis and immunotherapy of intrahepatic cholangiocarcinoma, Front. Oncol. 11 (2021) 757919.
[26] W. Roh, P.L. Chen, A. Reuben, C.N. Spencer, P.A. Prieto, J.P. Miller, et al., Integrated molecular analysis of tumor biopsies on sequential CTLA-4 and PD-1 blockade reveals markers of response and resistance, Sci. Transl. Med. 9 (379) (2017).
[27] Y. Hoshida, J.P. Brunet, P. Tamayo, T.R. Golub, J.P. Mesirov, Subclass mapping: identifying common subtypes in independent disease data sets, PLoS One 2 (11) (2007) e1195.
[28] S.L. Topalian, J.M. Taube, R.A. Anders, D.M. Pardoll, Mechanism-driven biomarkers to guide immune checkpoint blockade in cancer therapy, Nat. Rev. Cancer 16 (5) (2016) 275–287.
[29] M.D. Xu, Y. Wang, W. Weng, P. Wei, P. Qi, Q. Zhang, et al., A positive feedback loop of lncRNA-PVT1 and FOXM1 facilitates gastric cancer growth and invasion, Clin. Cancer Res. : an official journal of the American Association for Cancer Research 23 (8) (2017) 2071–2080.
[30] A. Bhan, M. Soleimani, S.S. Mandal, Long noncoding RNA and cancer: a new paradigm, Cancer Res. 77 (15) (2017) 3965–3981.
[31] S. Henderson, T. Fenton, APOBEC3 genes: retroviral restriction factors to cancer drivers, Trends Mol. Med. 21 (5) (2015) 274–284.
[32] B.E. Lippitz, Cytokine patterns in patients with cancer: a systematic review, Lancet Oncol. 14 (6) (2013) e218–e228.
[33] K.L. Owen, N.K. Brockwell, B.S. Parker, JAK-STAT signaling: a double-edged sword of immune regulation and cancer progression, Cancers 11 (12) (2019).
[34] G.H. Williams, K. Stoeber, The cell cycle and cancer, J. Pathol. 226 (2) (2012) 352–364.
[35] N.M. Anderson, P. Mucka, J.G. Kern, H. Feng, The emerging role and targetability of the TCA cycle in cancer metabolism, Protein Cell 9 (2) (2018) 216–237.
[36] H. Gaillard, T. García-Muse, A. Aguilera, Replication stress and cancer, Nat. Rev. Cancer 15 (5) (2015) 276–289.
[37] R. Moradi-Marjaneh, S.M. Hassanian, H. Fiuji, S. Soleimanpour, G.A. Ferns, A. Avan, et al., Toll like receptor signaling pathway as a potential therapeutic target in colorectal cancer, J. Cell. Physiol. 233 (8) (2018) 5613–5622.
[38] T.T. Wang, Y.L. Zhao, L.S. Peng, N. Chen, W. Chen, Y.P. Lv, et al., Tumour-activated neutrophils in gastric cancer foster immune suppression and disease progression through GM-CSF-PD-L1 pathway, Gut 66 (11) (2017) 1900–1911.
[39] S. Urakawa, M. Yamasaki, K. Goto, M. Haruna, M. Hirata, A. Morimoto-Okazawa, et al., Peri-operative monocyte count is a marker of poor prognosis in gastric cancer: increased monocytes are a characteristic of myeloid-derived suppressor cells, Cancer Immunol. Immunother. 68 (8) (2019) 1341–1350.
[40] F. Xu, H. Zhang, J. Chen, L. Lin, Y. Chen, Immune signature of T follicular helper cells predicts clinical prognostic and therapeutic impact in lung squamous cell carcinoma, Int. Immunopharm. 81 (2020) 105932.
[41] B.Z. Qian, J.W. Pollard, Macrophage diversity enhances tumor progression and metastasis, Cell 141 (1) (2010) 39–51.
[42] M. Lv, M. Chen, R. Zhang, W. Zhang, C. Wang, Y. Zhang, et al., Manganese is critical for antitumor immune responses via cGAS-STING and improves the efficacy of clinical immunotherapy, Cell Res. 30 (11) (2020) 966–979.
[43] L. Zhang, Y. Liu, F. Song, H. Zheng, L. Hu, H. Lu, et al., Functional SNP in the microRNA-367 binding site in the 3'UTR of the calcium channel ryanodine receptor gene 3 (RYR3) affects breast cancer risk and calcification, Proc. Natl. Acad. Sci. U.S.A. 108 (33) (2011) 13653–13658.
[44] F. Li, Z. Fang, J. Zhang, C. Li, H. Liu, J. Xia, et al., Identification of TRA2B-DNAH5 fusion as a novel oncogenic driver in human lung squamous cell carcinoma, Cell Res. 26 (10) (2016) 1149–1164.
[45] A.K. Murugan, A.K. Munirajan, N. Tsuchida, Genetic deregulation of the PIK3CA oncogene in oral cancer, Cancer Lett. 338 (2) (2013) 193–203.
[46] F. Mosele, B. Stefanovska, A. Lusque, A. Tran Dien, I. Garberis, N. Droin, et al., Outcome and molecular landscape of patients with PIK3CA-mutated metastatic breast cancer, Ann. Oncol. : Off. J. Eur. Soc. Med. Oncol. 31 (3) (2020) 377–386.
[47] W. Zhang, R. Hong, L. Xue, Y. Ou, X. Liu, Z. Zhao, et al., Piccolo mediates EGFR signaling and acts as a prognostic biomarker in esophageal squamous cell carcinoma, Oncogene 36 (27) (2017) 3890–3902.
[48] P.L. Zhou, Z. Wu, W. Zhang, M. Xu, J. Ren, Q. Zhang, et al., Circular RNA hsa_circ_0000277 sequesters miR-4766-5p to upregulate LAMA1 and promote esophageal carcinoma progression, Cell Death Dis. 12 (7) (2021) 676.
[49] A.J. Sutton, N.J. Cooper, K.R. Abrams, P.C. Lambert, D.R. Jones, A Bayesian approach to evaluating net clinical benefit allowed for parameter uncertainty, J. Clin. Epidemiol. 58 (1) (2005) 26–40.
[50] R.C. Montenegro, A. Howarth, A. Ceroni, V. Fedele, B. Farran, F.P. Mesquita, et al., Identification of molecular targets for the targeted treatment of gastric cancer using dasatinib, Oncotarget 11 (5) (2020) 535–549.
[51] M. Shi, B. Lou, J. Ji, H. Shi, C. Zhou, Y. Yu, et al., Synergistic antitumor effects of dasatinib and oxaliplatin in gastric cancer cells, Cancer Chemother. Pharmacol. 72 (1) (2013) 35–44.
[52] Y. Ye, O. Ge, C. Zang, L. Yu, J. Eucker, Y. Chen, LINC01094 predicts poor prognosis in patients with gastric cancer and is correlated with EMT and macrophage infiltration, Technol. Cancer Res. Treat. 21 (2022 Jan-Dec) 15330338221080977.